The Forward Detectors of CDF and DØ

Konstantin Goulianos

The Rockefeller University, 1230 York Avenue, New York, NY 10065-9965, USA

DOI: will be assigned

The forward detectors of CDF II are presented with emphasis on design aspects that proved crucial for carrying out a successful program on diffraction at the Tevatron. Alignment, calibrations and backgrounds are discussed, pointing out their relevance to the diffractive and central exclusive production physics programs planned at the LHC. The DØ forward detectors, which with forward spectrometer on both the $\bar{p}$ and p sides offer the opportunity for a program complementarity to that of CDF are briefly presented for completeness.

1 Introduction

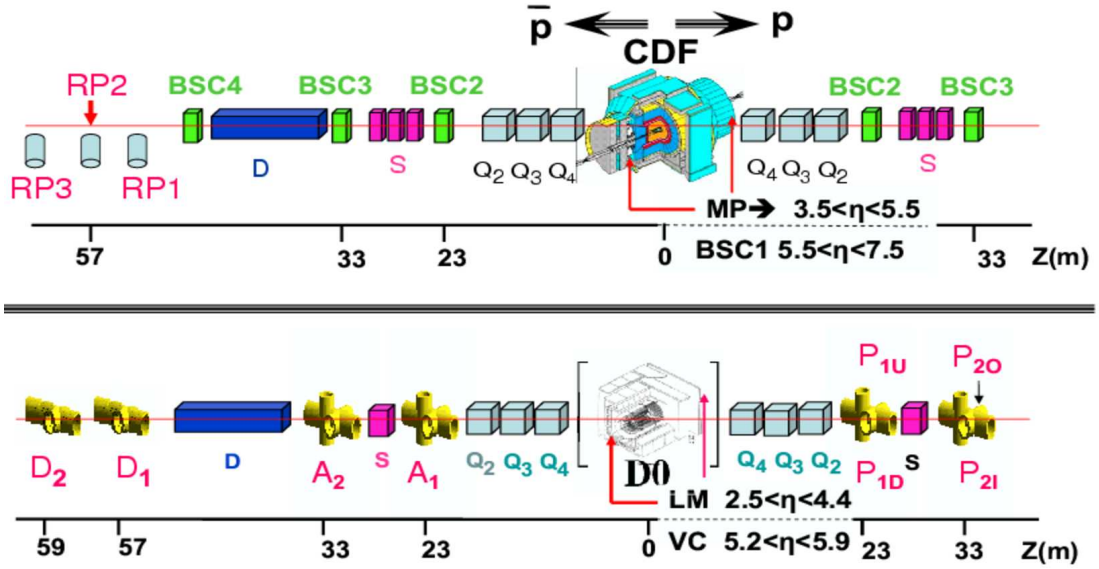

Figure 1: The CDF and D0 detectors in Run II

The Collider Detector at Fermilab (CDF) and the DØ collaborations have been conducting studies in diffraction since the start of Tevatron operations in 1989. A plethora of results have been obtained on forward, central, and multi-gap diffraction processes, as well as on central exclusive production which is of special interest as it serves to calibrate theoretical models for exclusive Higgs boson production st the Large Hadron Collider (LHC). In this paper, we present the CDF II (CDF in Run II) and DØ forward detector configurations in Run II of the Tevetron $\bar{p}p$ collider and discuss issues of alignment, calibrations, backgrounds and physics reach.

The CDF II diffractive physics data were collected with an upgraded CDF detector, which included the following forward components [1] (see Figs. 1, 2):

– **Roman Pot Spectrometer (RPS)** to detect leading **antiprotons**,
– **MiniPlug (MP)** forward calorimeters covering the region $\sim 3.5 < |\eta| < 5.5$,
– **Beam Shower Counters (BSC)** around the beam pipe at $\sim 5.5 < |\eta| < 7.5$,
– **Cerenkov Luminosity Counters (CLC)** covering the range $\sim 3.7 < |\eta| < 4.7$.

The Roman Pot Spectrometer was the same one that was used in Run Ic [2]. It consists of X-Y scintillation fiber detectors [1] placed in three Roman Pot (RP) stations located at an average distance of 57 m downstream in the $\bar{p}$ direction. The detectors have a position resolution of $\pm 100\,\mu m$, which makes possible a $\sim 0.1\%$ measurement of the $\bar{p}$ momentum. In Run Ic, the $\bar{p}$-beam was behind the proton beam as viewed from the RPS side. An inverted polarity (with respect to Run I) of the electrostatic beam separators enabled moving the RPS detectors closer to the $\bar{p}$-beam and thereby gain acceptance for small $|t|$ down to $\xi \equiv 1 - x_F(\bar{p}) = 0.03$. For larger $|t|$, the values of ξ that can be reached are lower.

The MiniPlug calorimeters were installed within the inner holes of the muon toroids. They consist of layers of lead plates immersed in liquid scintillator. The scintillation light is collected by wavelength shifting fibers strung through holes in the lead plates and read out by multi-channel photomultiplier tubes (MCPMT's). The calorimeter *tower* structure is defined by arranging fibers in groups to be read out by individual MCPMT pixels. There are 84 towers in each MiniPlug measuring energy and position for both electromagnetic (EM) and hadron showers [3].

The Beam Shower counters are rings of scintillation counters *hugging* the beam pipe. The BSC-1 rings are segmented into four quadrants, while the other BSC's are segmented into two halves. These counters are used to provide:

(a) rapidity gaps triggers,
(b) *exclusivity* constraints in studies of exclusive production, and
(c) beam losses, by gating the $\mathrm{BSC2}_{\bar{p}}$ ($\mathrm{BSC2}_{\bar{p}}$) signal to the passage of the p ($\bar{p}$) beam.

The Cerenkov Luminosity Counters comprise a finely segmented system of gas Cerenkov counters pointing to the interaction point (I) and are normally used by CDF to measure the number of inelastic collisions per beam-beam bunch crossing and thereby the luminosity. In the diffractive program, they are used in the rapidity gap definition by detecting charged particles that might penetrate the MP calorimeters producing a signal too small to be detected above the MP tower thresholds used. Their high efficiency for detecting charged particles provides a valuable complementary input to that of the MP calorimeters.

The DØ Run II forward detectors include two *state of the art* Forward Proton Detector (FPD) spectrometers on the outgoing p and $\bar{p}$ directions equipped with X-Y-V silicon based trackers capable of resolving ambiguities in events with multiple tracks at high luminosities. The beam-line configuration on the $\bar{p}$-side is similar to that of CDF; however, the p-side spectrometer has no dipole magnets between the IP and the spectrometer, which restricts access to low-t recoil protons. In contrast, the MiniPlug based system of CDF allows access to low$t$ events but is not capable of measuring angular ϕ-correlations between the outgoing p and $\bar{p}$, which are important for certain physics studies.

The CDF II [4] and DØ [5] detector layouts are schematically shown and compared in Fig. 1.

[1] We use a coordinate system with origin at the center of the CDF detector, Z along the proton beam direction and Y pointing up; the X coordinate points away from the center of the accelerator ring.

2 Alignment

A precise alignment of the RPS detectors is crucial for an accurate determination of the ξ and t values of the recoil antiproton. The standard alignment method based on surveying the detectors relative to the centerline of the beam pipe and using beam position monitors (BPM) to determine the beam position relative to the center of the pipe was hampered in Run II by several difficulties, including:

- there was no BPM in the vicinity of the RPS detectors;
- the beam position and angle could change with beam store as a result of tuning to increase the luminosity, and also during the course of a store;
- the position of the RP relative to the beam pipe could also change relative to the surveyed position due to slippage of the positioning mechanism.

The RPS alignment was addressed in CDF by developing a *dynamic alignment* method in which the actual detector position during data taking is determined from the recorded data. The method is based on the expectation that the t-distribution of the recoil antiproton be maximal at $|t| = 0$. However, the measured distribution will display such a maximum only if the detectors are correctly aligned. This is illustrated in Figs. 2, 3, 4. In practice, offsets in the X and Y coordinates of the RPS detectors with respect to the beam line are introduced in the off-line analysis and iteratively adjusted until a maximum for $d\sigma/dt|$ is obtained at $|t| = 0$. Using the resulting values for $X_{\rm offset}$ and $Y_{\rm offset}$ corresponds to having aligned detectors. This method is very precise and only limited by the statistics of the event sample, the size of the beam, and the jitter in the beam position during data taking of the particular data sample used. Using a special data sample collected during a relatively short dedicated run an accuracy of ± 30 μm in beam position was obtained [6].

The dynamic alignment method is quite general and can equally well be used to accurately calibrate the position of RPS detectors planned for the LHC. In principle, the offsets could be determined from small data samples and applied on-line during data taking to enrich the recorded data sample with useful events.

3 Calibrations and backgrounds

3.1 Missing forward momentum and W mass from diffractive events

A well known and frequently used data analysis tool is missing transverse energy. This tool is particularly useful in cases involving neutrinos in the final state. A good example is the determination of the mass of the W-boson through the $W \to e\nu$ / $\mu\nu$ decay modes. The usual technique is to use the *transverse* W mass, which results is a skewed distribution that requires Monte Carlo and detector simulations that affect the accuracy of the measurement. The detection in the RPS of the forward $\bar{p}$ in diffractive W production makes possible the determination of the full kinematics of the $W \to e\nu/\mu\nu$ decay.

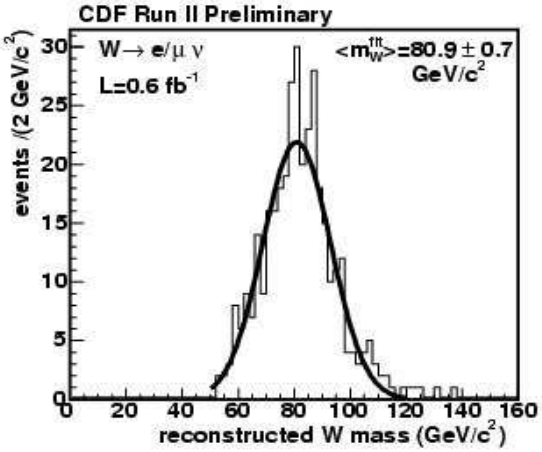

Figure 5: Diffracive W mass and Gaussian fit.

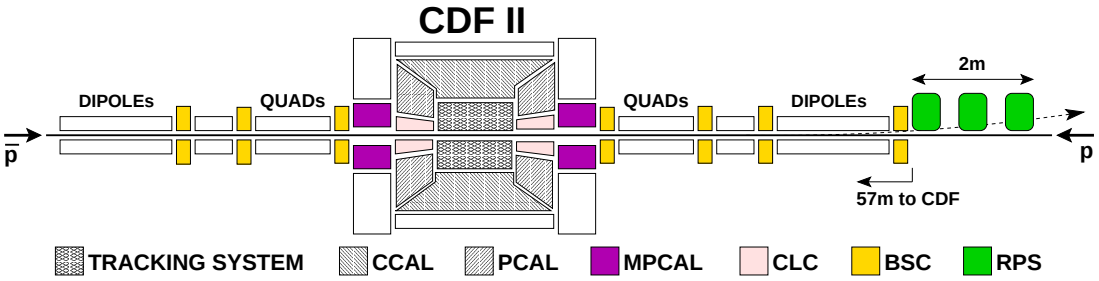

Figure 2: Schematic drawing of the CDF II detector (not to scale)

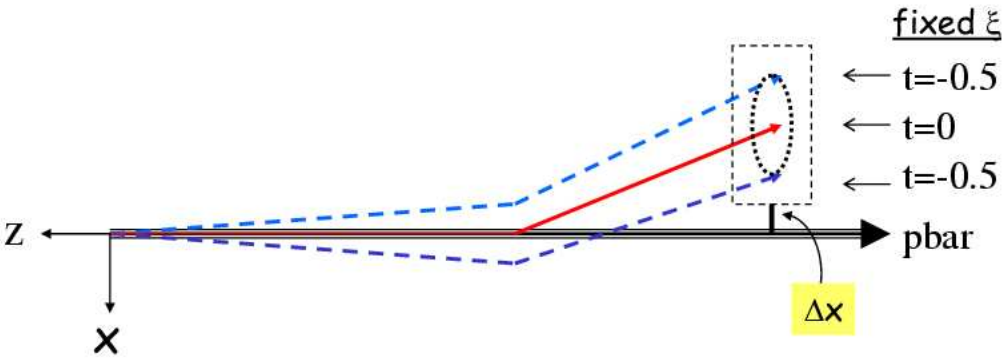

Figure 3: Schematic representation of a track detected by the RPS.

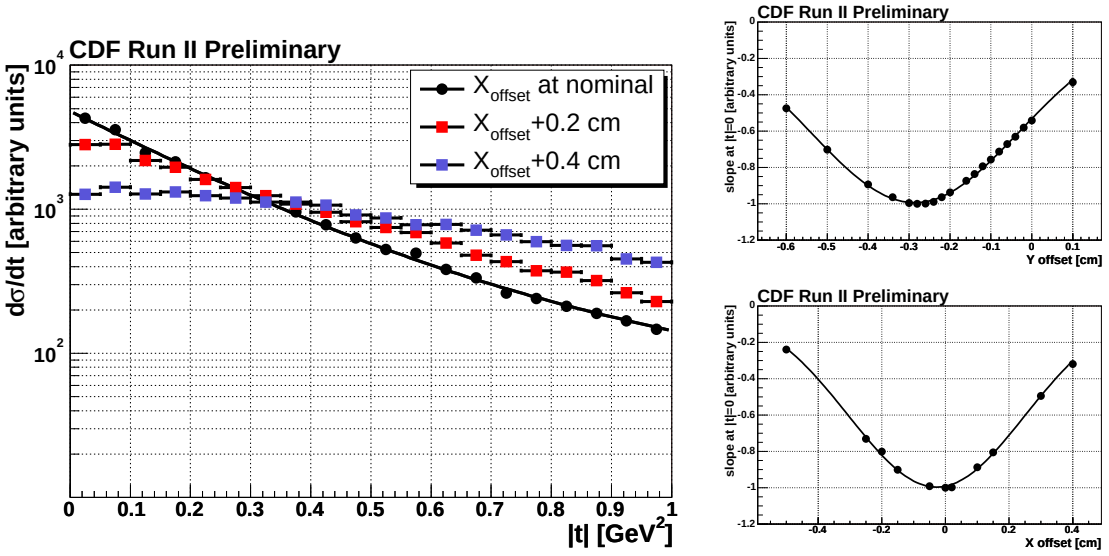

Figure 4: *Left*: t-distribution of reconstructed RPS tracks for positive X_{offset} shifts; *Right*: $|b|$ slope versus Y (*top*) and X (*bottom*) offsets.

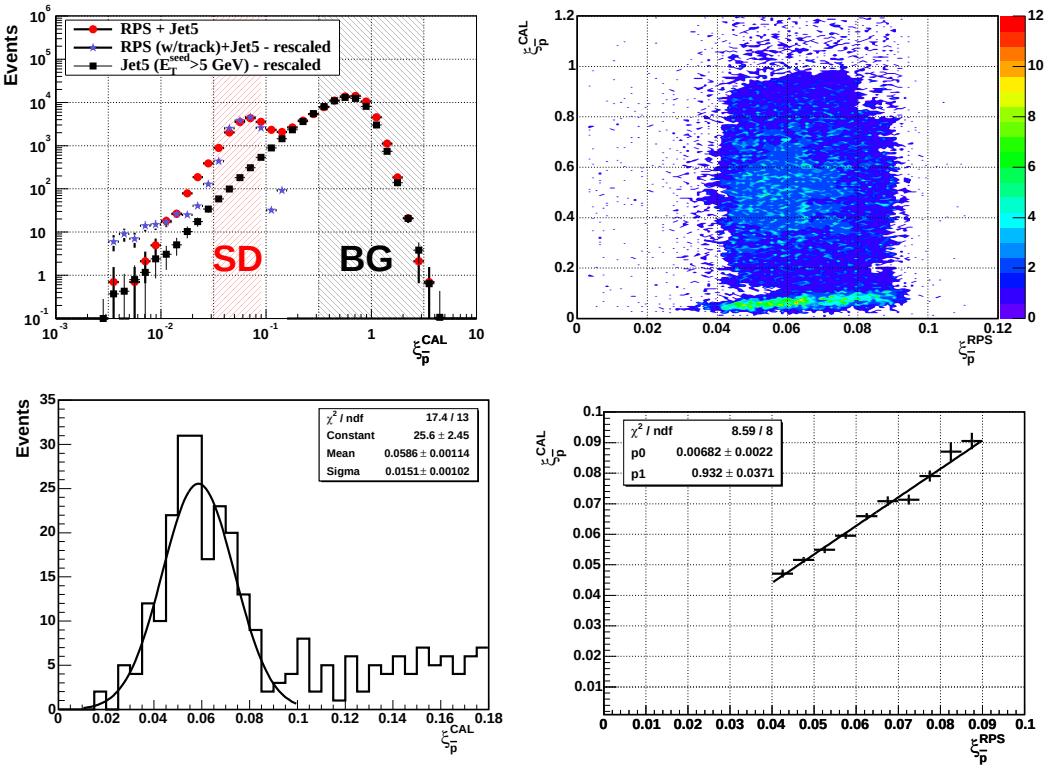

Figure 6: $\xi_{\bar{p}}^{CAL}$ vs. $\xi_{\bar{p}}^{RPS}$ (see text): *(t-l)* $\xi_{\bar{p}}^{CAL}$ distributions; *(t-r)* 2D-distribution of $\xi_{\bar{p}}^{CAL}$ vs. $\xi_{\bar{p}}^{RPS}$; *(b-l)* ξ^{CAL} for a slice of the 2D-dist. of $0.055 < \xi_{\bar{p}}^{RPS} < 0.060$; *(b-r)* $\xi_{\bar{p}}^{CAL}$ vs. $\xi_{\bar{p}}^{RPS}$.

The neutrino transverse energy E_T^{ν} is obtained from the missing E_T, as usual, and the pseudorapidity η_ν from the formula $\xi_{\bar{p}}^{\rm RPS}$-$\xi^{\rm cal} = (E_T/\sqrt{s})\exp[-\eta_\nu]$, where $\xi^{\rm cal}$ is calculated from the calorimeter towers: $\xi_{\bar{p}}^{\rm cal} = \Sigma_{\rm i-towers}(E_T^{\rm i}/\sqrt{s})\cdot\exp[-\eta_i]$. This method has been applied to CDF data yielding the preliminary result shown in Fig. 5. Using a data sample of ~ 300 diffractive W events, CDF obtained $M_W^{\rm exp} = 80.9 \pm 0.7$ GeV [7] in good agreement with the world average W-mass of $M_W^{\rm PDG} = 80.403 \pm 0.029$ GeV [8].

3.2 Overlap background and $\xi_{\bar{p}}^{\rm CAL}$ calibration

The main event sample of diffractive events in Run II was collected without RPS tracking information. For these events, $\xi_{\bar{p}}$ was evaluated from calorimeter information using the formula:

$$\xi_{\bar{p}}^{\rm CAL} = \Sigma_{\rm i-towers}(E_T^{\rm i}/\sqrt{s})\cdot\exp[-\eta_i].$$

The calorimeter based $\xi^{\rm CAL}$ was calibrated against ξ^{RPS} using a data sub-sample for which tracking was available. In implementing the calibration procedure, special care had to be taken to handle the background from overlap events at the high instantaneus luminosity ($\mathcal{L}$) of the run. Figure 6 illustrates the overlap background handling and the $\xi^{\rm CAL}$ vs. $\xi^{\rm RPS}$ calibration.

3.2.1 Overlap background

The $\xi_{\bar{p}}^{\rm CAL}$ distribution is shown in Fig. 6 for three diffractive dijet data samples defined in the insert. A *single-vertex* requirement was applied to all samples. The region indicated as SD contains events which are mostly due to single-diffractive (SD) dijet production, while the events in the ND region are mainly overlaps of a non-diffractive (ND) dijet and a soft diffractive interaction that triggered the RPS but yielded no reconstructed vertex. The majority of the diffractive events are represented by the excess of events of the RPS·Jet5 over the rescaled Jet5 distribution in the SD region. The overlap background in the region $0.03 < \xi_{\bar{p}}^{\rm CAL} < 0.09$ is of $\mathcal{O}(10\%)$.

Figure 6 *(t-r)* shows a two-dimensional scatter plot of $\xi_{\bar{p}}^{\rm CAL}$ vs. $\xi_{\bar{p}}^{\rm RPS}$ for the events with a reconstructed RPS track. The mountain-like peak in the region of $\xi_{\bar{p}}^{\rm CAL} \lesssim 0.1$ is attributed to diffractive events. The events with $\xi_{\bar{p}}^{\rm CAL} > 0.1$ are mostly due to ND dijets with a superimposed soft SD overlap event.

3.2.2 $\xi_{\bar{p}}^{\rm CAL}$ calibration

The calibration of of $\xi_{\bar{p}}^{\rm CAL}$ is performed by dividing the data into bins of width $\Delta\xi_{\bar{p}}^{\rm RPS} = 0.005$ and fit the $\xi_{\bar{p}}^{\rm CAL}$ values in each bin with a Gaussian distribution excluding the now well separated background, as shown in Fig. 6 *(b-l)* for $0.055 < \xi_{\bar{p}}^{\rm CAL} < 0.060$. The ratio of the half-width average of the fitted curve is $\delta\xi_{\bar{p}}^{\rm CAL}/\xi_{\bar{p}}^{\rm CAL} \approx 0.3$. Figure 6 *(b-r)* shows the results for the region $0.04 < \xi_{\bar{p}}^{\rm RPS} < 0.09$. A linear relationship is observed between $\xi_{\bar{p}}^{\rm CAL}$ and $\xi_{\bar{p}}^{\rm RPS}$ in this region.

4 Summary

The CDF and DØ forward detectors designed and used for studies of diffraction in Run II at the Ferrmilab Tevatron $\bar{p}p$ collider were presented with a focus on issues of alignment, calibrations, backgrounds and physics reach. The procedures developed are quite general can be directly adapted to the experiments planning diffractive physics studies at the LHC.

References

[1] A. Aaltonen *et al.* (CDF Collaboration), *Observation of Exclusive Dijet Production at the Fermilab Tevatron $\bar{p}p$ Collider,* Phys. Rev. D77:052004, 2008. DOI : 10.1103/PhysRevD.77.052004. Report number: FERMILAB-PUB-07-647-E.

[2] H. Nakada, Ph.D. thesis, University of Tsukuba, January 2001.

[3] K. Goulianos, M. Gallinaro, K. Hatakeyama, S. Lami, C. Mesropian, A. Solodsky, *The CDF Miniplug Calorimeters (and references therein),* Nucl. Instrum. Methods A **496**, 333 (2003).

[4] D. Acosta *et al.* (CDF Collaboration, Phys. Rev. **D** 71, 232001 (2005).

[5] DØ Collacoration, *The Upgraded D0 Detector,* arXiv:physics/0507191v2.

[6] Michele Gallinaro, DIS-2006, arXiv:hep-ex/0606024.

[7] K. Goulianos, *Diffractive W and Z production at Tevatron* arXiv:0905.4281v2 [hep-ex]; paper resented for the CDF collaboration at XLIVth Rencontrès de Moriond, QCD and High Energy Interactions, La Thuile, Aosta Valley, Italy, March 14-21, 2009.

[8] W.-M. Yao et al., Journ. Phys. G **33**, 1 (2006) and 2007 partial update for 2008, http://pdg.lbl.gov.